Modeling of Steel Reinforced Ultra-High-Performance Concrete (UHPC) Beams Failure

Tathagata Bhaduri[1] , Mohammed Alnaggar[2]

Authors & Affiliation:
[1] PhD Candidate, Department of Civil and Environmental Engineering, Rensselaer Polytechnic Institute, 110 8th St, Troy, NY 12180 USA. E-mail: bhadut@rpi.edu
[2] Assistant Professor, Department of Civil and Environmental Engineering, Rensselaer Polytechnic Institute, 110 8th St, Troy, NY 12180 USA. E-mail: alnagm2@rpi.edu

Abstract:
Ultra-high performance concrete (UHPC) is a cementitious composite with compactly graded mix capable of attaining a very high compressive strength (around 150 MPa) as well as superior ductility when mixed with fiber reinforcements. Due to the complex composition of reinforced UHPC beams (cementitious matrix, fibers, and regular reinforcement), it is very challenging to predict its mechanical and damage behavior by developing empirical or semi-empirical prediction models. Therefore, the current study aims at employing a comprehensive computational model to predict the performance of reinforced UHPC beams with varying fiber contents while explaining the failure mode transitions from diagonal shear (without fibers) to flexural failure as fiber volume increases. The lattice discrete particle model with fibers (LDPM-F) is utilized in the current investigation to virtually probe into the reinforced UHPC beams to understand their failure characteristics. LDPM-F effectively accounts for concrete heterogeneity and intricate quasi-brittle features with mechanics of bond-slip for random fibers distribution. In the current scope of the study, LDPM-F is briefly reviewed and parameter identification assumptions are discussed to increase the robustness of the calibration. Results from an experimental program executed by other members of the same research group are simulated in this study. Experiments consisted of flexural testing of reinforced UHPC beams with varying fiber contents along with splitting, uniaxial compression and notched three-point bending tests of companion samples taken from the same batches from which the beams were cast. Calibration is performed using these companion specimens and the responses of beams are used for validation. Excellent agreement is observed in predicting the transition of failure modes and crack localization for different experimental test cases of reinforced UHPC beams. Moreover, this computational model enables virtual testing of the beams to explore the relative contributions of different load transfer mechanisms in the beam during failure showing the extent of fiber bridging, matrix damage and their interplay with reinforcement.

1. Introduction

Ultra-high performance concrete (UHPC) is an advanced category material among cementitious composites which has optimally designed particle packing, capable of exhibiting high compressive strength >150 MPa (21.75 ksi) and significantly large post-cracking tensile capacity >5 Mpa (0.725 ksi) [Graybeal,2006] compared to conventional concrete. Following the increased popularity of UHPC in the past few years, there is a rise in research efforts to understand the potential advantages of this material as well as developing reliable design guides for structural applications. One of the major design criteria for structures is shear failure mode, which is characterized to be brittle and catastrophic in nature for conventional reinforced concrete beams. In this regard, there is a significant amount of research corresponding to fiber-reinforced concrete (FRC) and high-performance concrete (HPC) for their structural behaviors in shear. However, an extrapolation or inference from those may lead to dubious conclusions for reinforced UHPC beams [Baby et al.,2013].

Lately, a few investigations have addressed the shear behavior of UHPC beams to bring about insights on different load-carrying phases of shear transfer [Graybeal,2006; Heggar and Bertram,2008; Voo et al.,2010; Baby et al.,2013; Qi et al.,2016; Meszoly and Randl,2018]. Additionally, an interim design recommendation by the French Association of Civil Engineering [AFGC-Setra,2013] is available for shear design of UHPC beams which is mostly based on semi-empirical prediction models. Nevertheless, only a handful of cases are available which have explored detailed modeling of reinforced UHPC beams behavior in shear quantifying the different contributions of failure mechanisms and their interplay. Yao et al.,(2018) applied a simplified closed form formulation [Mobasher et al.,2015] based on relevant homogenized constitutive laws of UHPC to analytically estimate the behavior of reinforced UHPC beams. This model doesn't take account for the effect of discrete fibers micro-mechanics explicitly. Another class of modeling involved classical finite element tools incorporating concrete damage plasticity (CDP) framework which showed good agreement in predicting flexural failure of UHPC beams [Singh et al.,2017]. Yin et al.,(2019) simulated the flexural behavior of reinforced UHPC beams using a similar concrete plasticity model and it showed reasonable accuracy in predicting the experimental outcomes. Although these models provide a decent experimental prediction, they are needed to be calibrated for new constitutive laws every time for assumed homogenized fiber reinforced UHPC matrix with specific fiber dosage, fiber geometry and also possible fiber orientation during the flow of matrix. Furthermore, classical macroscale finite elements are unable to capture the rich lower scale events to reliably provide meaningful intuitions on the interplay of different reinforcing constituents.

To bridge this knowledge gap, the current study is conducted using lattice discrete particle model (LDPM) for fibers (LDPM-F) [Cusatis et al.,2011, Schauffert and Cusatis,2011]. LDPM-F had been instrumental in simulating concrete heterogeneity and multi-axial cracking and damage behavior in the presence of fibers. In this context, this model is calibrated and validated for reinforced UHPC beams with different fiber contents and reinforcement ratio based on a set of comprehensive experimental investigation performed by other members of the same research group at Rensselaer. The calibrated model showed the efficacy of this approach in accurately capturing different failure modes to furnish a key knowledge on the coupled participation of two different length scales of reinforcements (fiber and rebar) on the damage behavior of reinforced UHPC beams.

2. Review of the Lattice Discrete Particle Model with Fibers (LDPM-F)

LDPM-F represents concrete class substances numerically at its mesoscale as a two-phase material (coarse aggregate and mortar matrix). The mesh is then generated by first, distributing spherical particles that replicate the actual aggregate particle size distribution which is provided through the concrete mix-design information. Then, the zero diameter nodes are placed on the boundaries to facilitate the application of boundary conditions. Next, Delaunay tetrahedralization between the centers of the nodes is used to generate the interacting lattice network. Finally, the lattice network internal volumes are divided using a modified Voronoi tessellation to force the interaction planes to pass between aggregate gaps and not through the aggregates. Interaction among particles is achieved by a vectorial stress-strain relationship. After generating the concrete geometry, fibers are also placed in the domain with either random or preferential orientations. Fiber contributions are added to the facets they pass through by imposing local strain compatibility. For more details, the reader is directed to the background formulation papers of LDPM-F [Cusatis et al.,2011; Schauffert and Cusatis,2011].

3. Numerical Simulations and Comparison with Experimental Data

To understand the extent and interactions of different load transfer mechanisms in reinforced UHPC beams, an experimental campaign was designed consisting of a series of reinforced UHPC beams with different fiber contents and reinforcement ratios. Companion specimens were also cast from the same beam batches. The UHPC material used was donated by Ductal®.

3.1 Calibration and Initial Validation Using Companion Specimens

First, Ductal® JS1000 mix design parameters are used to generate the geometric mesh which consisted of binder content $b = 943$ Kg/m^3 (58.87 lb/ft^3), Water-to-binder ratio $w/b = 0.138$, and aggregate-to-binder ratio a/b= 1.305. The actual maximum aggregate size was 0.6 mm (0.023 in.). Since aggregate pieces represent the computational nodes, the smaller they are within a specific volume, the higher the number of degrees of freedoms which will cause large computational cost. Although the companion samples can be simulated within a reasonable amount of computational time using the actual maximum aggregate size, previous research using LDPM-F for UHPC has shown that using a coarse-grained version of the mesh with maximum aggregate size of 4 mm also yields very reasonable results [Smith et al.,2014;Wan et al.,2016;Rafiq,2016]. So, the aggregate parameters used to generate the geometry were selected to be: maximum aggregate size $d_a = 4$ mm (0.157 in.); minimum aggregate size $d_0 = 2$ mm (0.078 in.); and Fuller exponent $n_F = 0.5$ [Rafiq,2016]. Steel fibers of 12.3 mm (0.48 in.) length and 0.2 mm (0.0078 in.) diameter were used for the mix. In the model, fibers are assumed to be straight and randomly placed with or without preferential directions.

In the next step, the matrix mechanical response is identified by using the results of tested companion specimens without fibers. In general, LDPM has seventeen parameters to fully describe the multi-axial concrete behavior. Yet, many of these parameters are needed to describe the confined behavior under multi-axial compressive stresses to represent pore collapse and material compaction. Under general flexural and shear behavior, as well as for uniaxial compression, it can be assumed that high confinements are not achieved. Therefore, previous researches [Alnaggar et al.,2018], as well as the original LDPM formulations [Cusatis et al.,2011], showed that

only five mesoscale parameters are sufficient to describe unconfined behavior in tension, compression, and shear. These parameters are: normal elastic modulus E_0, shear normal coupling parameter α, mesoscale tensile strength σ_t, tensile characteristic length l_t and mesoscale shear strength σ_s. Therefore, these five parameters are only calibrated and the rest of the parameters are assumed based on previous literature as following: initial friction $\mu_0 = 0.15$, asymptotic friction $\mu_\infty = 0$, transitional stress $\sigma_{N0} = 600$ MPa (87 ksi), yielding compressive strength $\sigma_{c0} = 150$ MPa (21.76 ksi), ratio of initial hardening modulus to normal modulus H_{c0}/E_0=0.6, softening coefficient n_t=0.2, transitional strain ratio k_{c0}=2, deviatoric strain threshold ratio k_{c1}=1, deviatoric damage parameter k_{c2}=5 [Alnaggar et al.,2018].

First, the material elastic behavior is captured by calibrating E_0 and α. This is done by fitting nominal stress-strain curves from the notched three-point bending tests (3PBT) without fibers to replicate the same macroscopic elastic modulus E. 3PBT tests were performed on 304.8 mm (12 in.) long beams with an effective span of 152.4 mm (6 in.) and a cross section of 50.8 mm (2 in.) $\times$ 50.8 mm (2 in.) having a notch height of 25.4 mm (1 in.). Nominal stress was computed as $\sigma_f = 3PL/2bh^2$ where P is applied vertical load, L is effective span, b is width, and h is depth of the specimen. Nominal strain was computed as $\varepsilon_f = CMOD/h$ where $CMOD$ is the crack mouth opening displacement. Since the tests did not include the measuring of ν, α =0.292 is assumed based on previous research [Rafiq,2016]. Finally, the fitting gives E_0 =90 GPa (13053.4 ksi). Using E_0 and α, the corresponding macroscopic elastic constants can be computed [Cusatis et al.,2011] as $E = 60.3$ GPa (8745.7 ksi) and $\nu = 0.165$. Both values match very well with the typically reported values in the literature [Russel and Graybeal,2013]. To identify the parameters representing fracture behavior, namely σ_t and l_t, the 3PBT results are used in combination with Brazilian splitting tests (BST). For regular strength concrete, BST gives a good approximation of its tensile strength [Alnaggar and Bhanot,2018]. However, for UHPC, secondary effects in BST including large damage under the loading platens, affect the tensile stress distribution. Therefore, both test results were simulated to achieve a reasonable coupled fitting of the two parameters. BST tests were done using 6 cylinders of diameter 50.8 mm (2 in.) and length 87.37 mm (3.44 in.). Nominal tensile stress was computed as $\sigma_t = 2P/\pi DL$ and nominal vertical strain was computed as $\varepsilon_t = \Delta/D$ where P, D, L and Δ denote applied load,diameter of specimen,length of specimen and vertical deformation along the width of the specimen. Finally, the calibration gives σ_t=18 MPa (2.61 ksi) and l_t=9.1 mm (0.36 in). Simulation results ("Num") for 3PBT and BST experimental scatter ("Expt") with average ("Expt Avg") are shown in Figure 1. One of the two replicas for the 3PBT without fibers was partially cracked during notch cutting, and therefore, the calibration targeted the higher peak as it is more reliable. Also, due to the high brittleness of the material without fibers, snapback was observed experimentally after the tensile peak in the 3PBT and that explains the straight line in the post-peak. Lastly, to calibrate σ_s, unconfined compression (UCC) test results (stress-strain data) of 6 cubes (0% fiber) with an edge length 50.8 mm (2 in.) are used and this gives σ_s =75.6 MPa (10.96 ksi). Numerical and experimental results are shown in Figure 1. The experimental campaign did not include fiber pullout tests, therefore, LDPM-F fiber parameters from a previous study [Rafiq,2016] are used since in this the same UHPC material was used. These are namely bond frictional stress τ_0=10 MPa (1.45 ksi), bond fracture energy G_d=0 J/m^2 (0 ft-lb/in^2) and slip hardening/softening parameter β=0. For steel fibers, the material and geometrical parameters are modulus of elasticity E_f=205 GPa (29732.74 ksi), ultimate tensile strength σ_{uf}=500 MPa (72.5 ksi), length L_f=13 mm (0.5 in.) and area A_f=0.0314 mm^2 (0.000048 in^2) [Rafiq,2016].
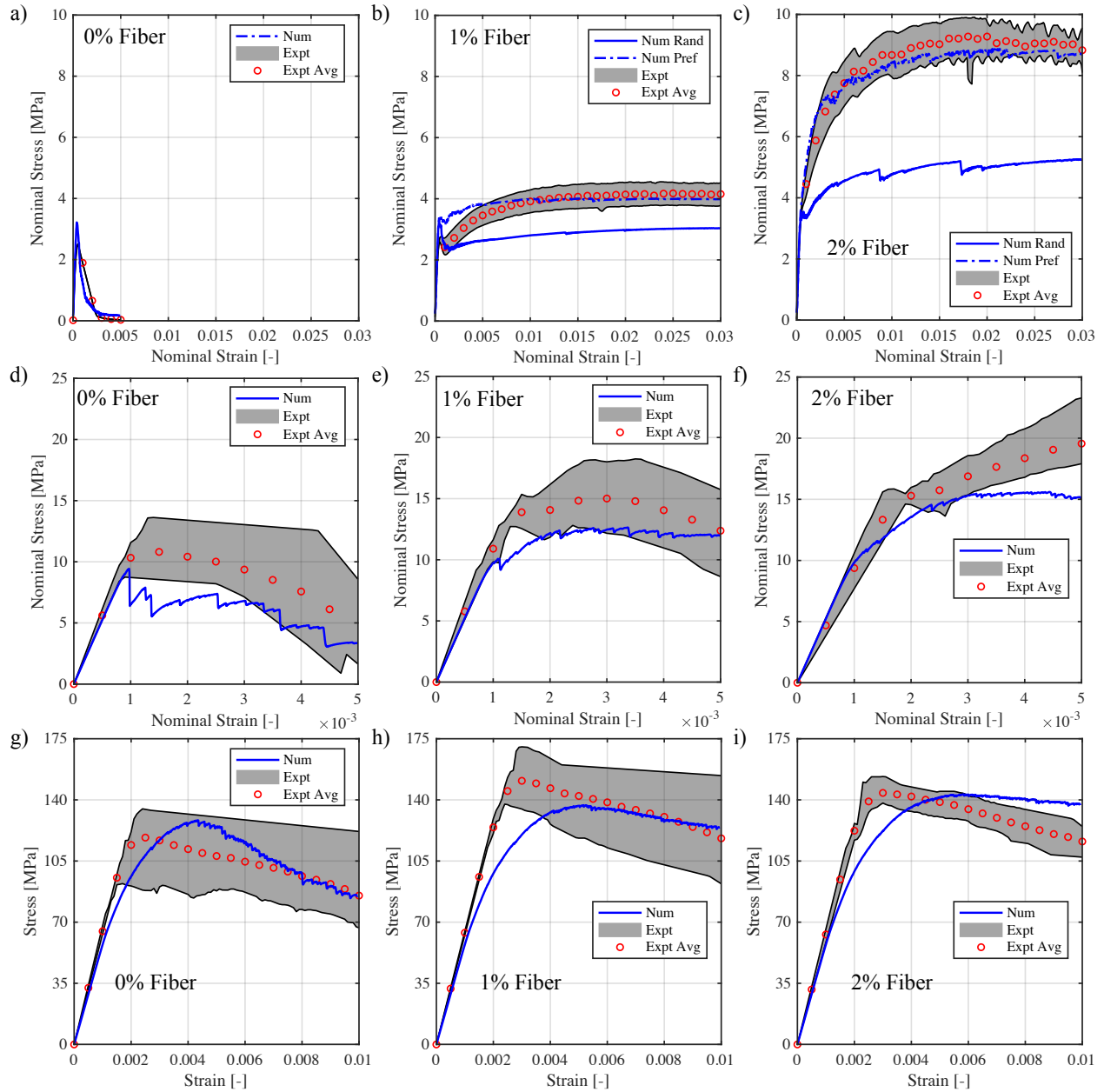
Figure 1: Calibration Results for: (a-c) 3 Point Bending Tests, (d-f) Brazilian Splitting Tests and, (g-i) Unconfined Compression Tests (1 MPa = 145 psi).

Using these calibrated parameters, simulations of the 3PBT, BST and UCC tests with 1% and 2% fiber contents by volume are performed as an initial validation at the material level (without considering the interaction with rebars). As can be seen for both the BST and UCC results, model predictions match fairly with the experimental data given its scatter. For the 3PBT, all samples were cast very slowly from one end and hence the material had to flow from one mold end to the other. So, it is expected that the fibers are partially oriented in the longitudinal direction due to the flow. Therefore, in generating the fibers, both random ("Rand") and preferential orientations ("Pref") of the fibers in the direction of flow are used. The numerical simulations also prove the

presence of a fiber preferential orientation as shown in Figure 1. The random cases show much lower capacities compared to the preferentially oriented ones. Nonetheless, this further indicates that LDPM-F can capture fiber orientation effects.

3.2 Prediction of Reinforced UHPC Beam Shear Behavior

After calibration, all model parameters are fixed and used to predict the behavior of 12 reinforced UHPC beams with different reinforcement and fiber contents in 3 point bending configuration. Four beams were cast from each of the three mixes with different fiber contents (0%, 1%, and 2%). For each fiber content group, #3 grade 60 rebars were used to reinforce two beams with one rebar and two other beams with two rebars. No stirrups were used. Beam dimensions and loading are shown in Figure 2a with LDPM-F modeling features. The point load is shifted from the center by 12.7 mm (0.5 in.) to force the shear failure to occur in one side of the beam. Rebars are modeled using a Timoshenko beam formulation with simple bi-linear steel constitutive law. Since the objective of this paper is to predict the interplay between fibers and longitudinal reinforcement, modeling of the rebar necking is not pursued. This is an acceptable choice since rebar necking occurs at a much higher strain compared to the fibers pull out strain. Therefore, the bi-linear fitting is performed to capture the yielding initiation and the initial strain hardening slope around 3% strain, which is much greater than fibers axial pull out strains [Duque and Graybeal,2017]. This gives a yield strength σ_y=482 MPa (69.91 ksi) and an initial hardening modulus E_{sh}=8900 MPa (1290.83 ksi). These values are obtained by fitting the experimental stress-strain curve of the used rebars. As can be seen from Figure 2b, the rebar model matches the experimental rebar test behavior quite well up to 0.03 strain (3%). This way, the interplay between fibers and rebar behavior at the onset of rebar yielding up to a small portion of its strain hardening can be captured. But at higher strains, the numerical model overestimates the rebar stress as can be seen at point **"P"** on the experimental curve for example. So, the following discussion of results only deals with the load-displacement history corresponding to rebar stresses only up to a maximum of 600 MPa (87 ksi) which corresponds to a rebar strain of about 3.8%. For each rebar/fiber content case, a point **"a"** on the numerical curves highlights a point at which, a snapshot of the failure pattern and rebar stress distribution is taken such that the rebar maximum stress is below 600 MPa (87 ksi) as shown in Figure 3. The following discussion of results is restricted to the beam behavior up to this point. Additionally, the bond between rebars and LDPM-F mesh is assumed to be perfect as suggested by the experimental results, and thus, a simple penalty constraint is used [Alnaggar et al.,2018]. Moreover, the loading and support platens, having the same dimensions of those used in the experiments, are modeled using hexahedral finite elements with elastic steel material properties. Also, in the simulations, fibers are placed with preferential orientations because the beams were also cast from one end. The simulated load-displacement responses for beams are shown in Figure 2.

From the results for the 0% fiber case (Figure 2c & f), the model captures the initial load drop at the onset of matrix brittle cracking, then it follows well the strength gain for both single and double rebar cases. The model also captures the correct failure mode as it predicts diagonal shear failure as can be seen from the initiation of large diagonal cracks in Figures 3a & d (final failure is not shown in the figures though). In addition, the model captures also the stages of failure. Notably, the beam with single rebar and 0% fiber (Figure 3a) started to fail by bending, then, due to strain hardening, the beam shear capacity was eventually reached and final failure was by diagonal shear. The model predicts this by showing that the rebar stress reaches 582 MPa (84.412 ksi) at point **"a"**
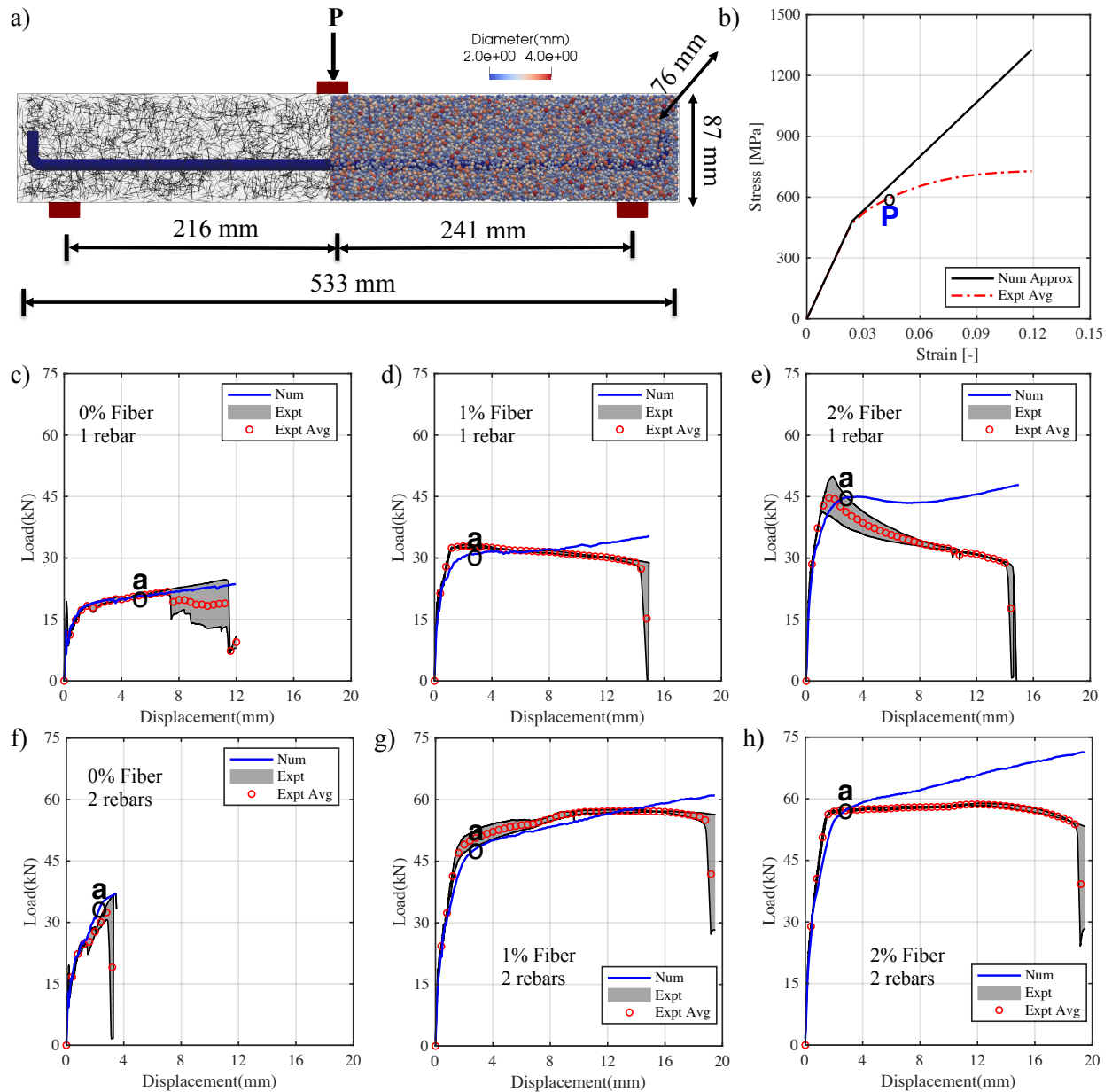
Figure 2: a) Beam model with dimensions, b) Rebar experimental and numerically simulated stress-strain curves, Three Point Bending test results for Reinforced UHPC Beams with (c-e) Single Rebar and, (f-h) Two Rebars (1 MPa = 145 psi, 1 kN = 225 lb, 25.4 mm = 1 in).

yet the load carrying capacity keeps increasing. For the two rebars case, the beam suddenly fails in shear at the onset of rebars yielding as shown in Figure 3d. This can also be proven by comparing the load-displacement slopes of the two beams in Figures 2c & f. Just after point **"a"** in Figure 2f, the beam fails experimentally, while at point **"a"** in Figure 2c, the beam continues to carry more loads. So, the model provides a measure of rebar stresses during and around failure.

For the beams with 1% fiber content (Figure 2d & g), the model also captures the onset of initial damage (see the change in response slope around 17 kN in both curves). At this point,

the rebars are not yielding but the fibers start to pull and crack bridging is initiated. With 1 rebar (Figure 2d), fibers are strong enough to bridge the cracks and force the rebar to yield at a localized zone. As a result, the experimental curve shows a negative slope after the first peak (around 1 mm displacement) and continues till it fails by rebar necking. This is captured indirectly by the model as it shows a plateau beyond point **"a"** corresponding to the exhausting of fibers only at a localized location followed by strain hardening (that we said is not realistic) that deviates from the experiments. With 2 rebars, (Figure 2g), the fibers can not restrict the two rebars and thus a more distributed yielding is evident but of course at a higher load. This is clear from the added ductility in the experiments but also at point **"a"**, the numerical simulations do show a higher slope compared to the single rebar case which means more fibers are contributing. In other words, the 2 rebars are forcing more cracks to open as the beam carries higher loads and thus more yielding locations are introduced. This can be more clearly shown by comparing crack distributions in Figures 3b & e where one can see more cracking extending in the case of 2 rebars. Collectively, the model captures the effect of fiber crack bridging on rebar yield localization. In addition, the model captures the forcing of multiple crack formations due to high steel reinforcement ratio.

This behavior is more evident in the case of 2% fiber content as shown in Figures 2e & h as well as Figures 3c & f. Similarly, in the load-displacement responses, the model shows a plateau at point **"a"** for 1 rebar and shows a continued strain hardening with 2 rebars. Yet, since fibers are more here, the single rebar yields in an even more localized manner as seen experimentally in Figure 2e which is numerically observed by comparing Figures 3b & c where at the same rebar maximum stress level, cracks and rebar stresses are more localized for the 2% case compared to the 1% case. Of course, with 2 rebars, the beam capacity is increased but it must be also noticed here that it is, in general, very similar to the 1% fiber case (see experimental peaks). While the model does not predict the peaks in both cases as they correspond to rebars necking (not considered in the model), yet it explains the difference by showing more distributed cracking in the 1% case with 2 rebars compared to 2% case with also 2 rebars as shown in Figures 3e & f. Not only that but as can be seen before point **"a"** for the two cases (Figures 2 g & h), the model captures the contribution of the additional fibers as the beam reaches a much higher peak at point **"a"**. This means that the additional fibers prevented the rebars from yielding and were carrying more loads even during initial crack bridging. In addition, more fibers meant that the rebars were forced to yield more locally compared to the 1% case which is evident from crack patterns. Nevertheless, at this point, 2% fibers is high enough to carry the loads and bridge the cracks as the rebars yield. When this is compared to the single rebar case, 2% fibers were very strong and forced the single rebar to neck very locally. One additional observation is very important from the design point of view which can be deduced by comparing 1% fibers with 2 rebars (Figure 2g) with 2% fibers with 1 rebar (Figure 2e). At point **"a"** in both figures, the beam capacity is nearly the same (about 45 to 47 kN) but from a ductility point of view, 1% fibers with 2 rebars is better. This is shown by comparing cracking where Figure 3e shows more distributed cracking and yielding compared to the other case (Figure 3c). This means that there exists a point at which, more fibers are not so beneficial compared to more reinforcement. It is also worth mentioning here the strong correlation between model crack pattern predictions and the final failure modes of the beams in all cases in Figure 3. For the cases without fibers, clear diagonal shear cracks are already formed. For cases with fibers, while the model crack patterns are at an early stage in failure, they all correspond to clear rebar yielding that involved multiple fiber crack bridging. This means that the model predicted cracks will not close after necking and unloading, and thus they do provide clues to the failure mode.
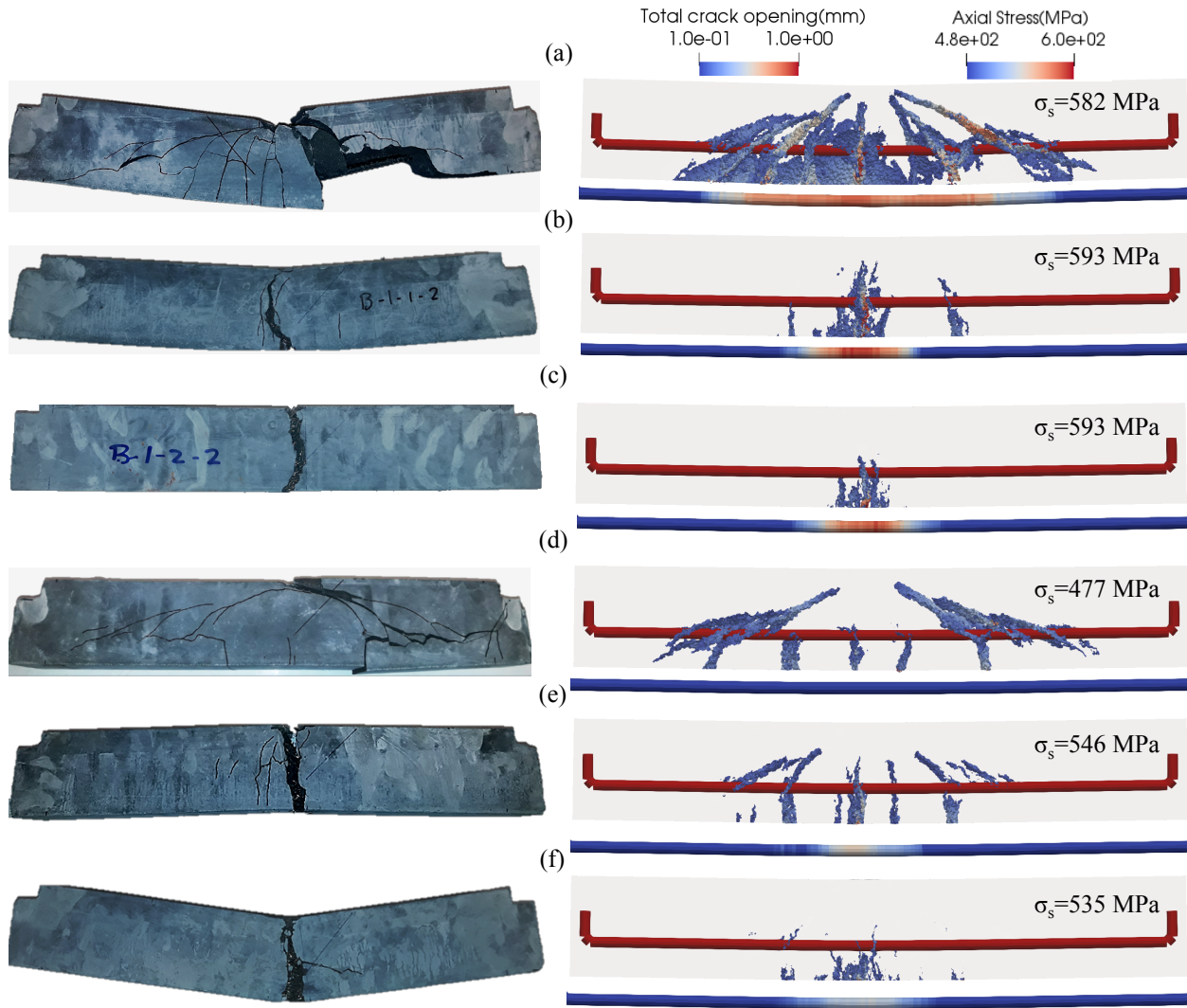
Figure 3: Experimental and numerical simulated failure pattern for: Beams with single rebar and fiber content of (a) 0%, (b) 1% and (c) 2%, and for beams with two rebars and fiber content of (d) 0%, (e) 1% and (f) 2% (1 MPa = 145 psi, 25.4 mm = 1 in).

5. Conclusions

This paper provides a calibrated and validated LDPM-F based numerical modeling of reinforced UHPC beam behavior under shear. Results show a clear interplay between fiber crack bridging and reinforcement ratio. As fibers increase, more crack closure is evident and the result is more localization in rebars yielding. As reinforcement increases, more cracks are forced to open and thus, more fiber crack bridging is seen. Results also show that fiber crack bridging/closure is very effective in preventing shear failure even without web reinforcement and at high rebar reinforcement ratios. Finally, by using this type of comprehensive modeling, the complex interactions between different mechanisms are easily investigated and quantified, and therefore, this modeling approach can be used to guide the formulation of design formulas to better account for coupled interactions between fibers and reinforcement.

6. References

AFGC, SETRA. "Bétons fibrés à ultra-hautes performances."Recommandations provisoires. Paris, (2013).

Alnaggar, Mohammed, and Naina Bhanot. "A machine learning approach for the identification of the Lattice Discrete Particle Model parameters." *Engineering Fracture Mechanics* 197 (2018): 160-175.

Alnaggar, Mohammed, Daniele Pelessone, and Gianluca Cusatis. "Lattice Discrete Particle Modeling of Reinforced Concrete Flexural Behavior." *Journal of Structural Engineering*145.1 (2018): 04018231

Baby, Florent, Pierre Marchand, and François Toutlemonde. "Shear behavior of ultrahigh performance fiber-reinforced concrete beams. II: Analysis and design provisions." *Journal of Structural Engineering* 140.5 (2013): 04013112.

Cusatis, Gianluca, Daniele Pelessone, and Andrea Mencarelli. "Lattice discrete particle model (LDPM) for failure behavior of concrete. I: Theory." *Cement and Concrete Composites* 33.9 (2011): 881-890.

Cusatis, Gianluca, et al. "Lattice discrete particle model (LDPM) for failure behavior of concrete. II: Calibration and validation." *Cement and Concrete composites* 33.9 (2011): 891-905.

Duque, Luis Felipe Maya, and Benjamin Graybeal. "Fiber orientation distribution and tensile mechanical response in UHPFRC." *Materials and Structures* 50.1 (2017): 55.

El Helou, Rafic Gerges. *Multiscale Computational Framework for Analysis and Design of Ultra-High Performance Concrete Structural Components and Systems.* Diss. Virginia Tech, 2016.

Graybeal, Benjamin A. "Structural Behavior of Ultra High Performance Concrete Prestressed I-Girders." (2006).

Graybeal, Benjamin A. *Material property characterization of ultra-high performance concrete.* No. FHWA-HRT-06-103. 2006.

Hegger, Josef, and Guido Bertram. "Shear carrying capacity of ultra-high performance concrete beams." *Proceedings, International fib Symposium, Amsterdam, The Netherlands in.* 2008.

Lale, Erol, et al. "Homogenization coarse graining (HCG) of the lattice discrete particle model (LDPM) for the analysis of reinforced concrete structures." *Engineering Fracture Mechanics* 197 (2018): 259-277.

Mészöly, Tamás, and Norbert Randl. "Shear behavior of fiber-reinforced ultra-high performance concrete beams." *Engineering Structures* 168 (2018): 119-127.

Mobasher, Barzin, Yiming Yao, and Chote Soranakom. "Analytical solutions for flexural design of hybrid steel fiber reinforced concrete beams." *Engineering Structures* 100 (2015): 164-177.

Qi, Jianan, Zhongguo John Ma, and Jingquan Wang. "Shear strength of UHPFRC beams: Mesoscale fiber-matrix discrete model." *Journal of Structural Engineering* 143.4 (2016): 04016209.

Russell, Henry G., and Benjamin A. Graybeal. *Ultra-high performance concrete: A state-of-the-art report for the bridge community*. No. FHWA-HRT-13-060. 2013.

Schauffert, Edward A., and Gianluca Cusatis. "Lattice discrete particle model for fiber-reinforced concrete. I: Theory." *Journal of Engineering Mechanics* 138.7 (2011): 826-833.

Singh, M., et al. "Experimental and numerical study of the flexural behavior of ultra-high performance fibre reinforced concrete beams." *Construction and Building Materials* 138 (2017): 12-25.

Smith, Jovanca, et al. "Discrete modeling of ultra-high-performance concrete with application to projectile penetration." *International Journal of Impact Engineering* 65 (2014): 13-32.

Voo, Yen Lei, Wai Keat Poon, and Stephen J. Foster. "Shear strength of steel fiber-reinforced ultrahigh-performance concrete beams without stirrups." *Journal of structural engineering* 136.11 (2010): 1393-1400.

Wan, Lin, et al. "Analysis of the behavior of ultra high performance concrete at early age." *Cement and Concrete Composites* 74 (2016): 120-135.

Xia, Jun, et al. "Shear failure analysis on ultra-high performance concrete beams reinforced with high strength steel." *Engineering Structures* 33.12 (2011): 3597-3609.

Yao, Yiming, et al. "Ultra high Performance Concrete-Materials Formulations and Serviceability based Design." *HAC 2018. V Congreso Iberoamericano de hormigón autocompactable y hormigones especiales.* Editorial Universitat Politècnica de València, 2018.

Yin, Hor, Kazutaka Shirai, and Wee Teo. "Finite element modelling to predict the flexural behavior of ultra-high performance concrete members." *Engineering Structures* 183 (2019): 741-755.

Yoo, Doo-Yeol, and Young-Soo Yoon. "Structural performance of ultra-high-performance concrete beams with different steel fibers." *Engineering Structures* 102 (2015): 409-423.